ChemPubSoc Europe

DOI: 10.1002/chem.201503991

CHEMISTRY A European Journal Full Paper

Photochemotherapeutics

# Upconverting Nanoparticles Prompt Remote Near-Infrared Photoactivation of Ru(II)–Arene Complexes

Emmanuel Ruggiero,[a] Claudio Garino,[b] Juan C. Mareque-Rivas,[a, c] Abraha Habtemariam,*[a, c, d] and Luca Salassa*[a, e]

*In memory of Jon Mikel Azpiroz*

**Abstract:** The synthesis and full characterisation (including X-ray diffraction studies and DFT calculations) of two new piano-stool $Ru^{II}$–arene complexes, namely $[(\eta^6\text{-}p\text{-cym})Ru(bpy)(m\text{-CCH-Py})][(PF)_6]_2$ (**1**) and $[(\eta^6\text{-}p\text{-cym})Ru(bpm)(m\text{-CCH-Py})][(PF)_6]_2$ (**2**; *p*-cym = *p*-cymene, bpy = 2,2′-bipyridine, bpm = 2,2′-bipyrimidine, and *m*-CCH-Py = 3-ethynylpyridine), is described and discussed. The reaction of the *m*-CCH-Py ligand of **1** and **2** with diethyl-3-azidopropyl phosphonate by Cu-catalysed click chemistry affords $[(\eta^6\text{-p-cym})Ru(bpy)(P\text{-Trz-Py})][(PF)_6]_2$ (**3**) and $[(\eta^6\text{-p-cym})Ru(bpm)(P\text{-Trz-Py})][(PF)_6]_2$ (**4**; P-Trz-Py = [3-(1-pyridin-3-yl-[1,2,3]triazol-4-yl)-propyl]phosphonic acid diethyl ester). Upon light excitation at $\lambda =$ 395 nm, complexes **1**–**4** photodissociate the monodentate pyridyl ligand and form the aqua adduct ions $[(\eta^6\text{-}p\text{-cym})Ru(bpy)(H_2O)]^{2+}$ and $[(\eta^6\text{-}p\text{-cym})Ru(bpm)(H_2O)]^{2+}$. Thulium -doped upconverting nanoparticles (UCNPs) are functionalised with **4**, thus exploiting their surface affinity for the phosphonate group in the complex. The so-obtained nanosystem **UCNP@4** undergoes near-infrared (NIR) photoactivation at $\lambda = 980$ nm, thus producing the corresponding reactive aqua species that binds the DNA-model base guanosine 5′-monophosphate.

## Introduction

Encouraged by the clinical success of photodynamic therapy (PDT),[1] light-activatable molecules and nanomaterials are being increasingly investigated for their capacity to generate biologically active species in situ with high spatiotemporal control. In principle, such an attractive strategy allows the biological effects of drugs to be localised, thus potentially reducing their therapeutic drawbacks. For this reason, light activation has found application in a number of fields and diverse systems have been designed as neuroscience tools,[2] drug delivery platforms,[3,4] and anticancer prodrugs.[5,6]

Promising metal-based photo-chemotherapeutics have been developed that exploit the unique photochemical and antitumor properties of transition-metal complexes. Several research groups worldwide have demonstrated that light-activatable complexes of various transition metals (e.g., Pt, Ru, Rh, and Ir) show encouraging antineoplastic profiles and unconventional mechanisms of action relative to their ground-state analogues.[4–7]

Nevertheless, the poor absorption properties of metal complexes in the therapeutic window of the red and near-infrared (NIR) spectrum (ca. $\lambda = 600$–1000 nm) pose a serious limitation to advancing their use toward preclinical and clinical studies because maximal light penetration into tissues is achieved in this wavelength range and damage to biological components is minimised.[8,9] Relative to PDT photosensitisers, photoactivatable anticancer metal complexes generally display low-energy absorption bands that rarely extend over $\lambda = 550$ nm and have modest extinction coefficients. Although a few exceptions have been reported,[10–12] it is extremely challenging to improve absorption features without altering the ground-state stability and photoreactivity of the metal complexes.

For this reason, we and other groups have recently started to explore the use of upconversion nanoparticles (UCNPs) as phototriggers for the NIR photoactivation of (anticancer) metal complexes.[9,13–20] UCNPs are typically $NaYF_4$ or $NaGdF_4$ nanocrystals doped with lanthanide ions, such as $Yb^{3+}$:$Tm^{3+}$ or $Yb^{3+}$:$Er^{3+}$, which convert NIR light ($\lambda = 980$ nm) into UV/Vis

[a] *E. Ruggiero, Prof. J. C. Mareque-Rivas, Dr. A. Habtemariam, Dr. L. Salassa*
*CIC biomaGUNE, Paseo de Miramón182*
*20009, Donostia-San Sebastián Euskadi (Spain)*
*E-mail: a.habtemariam@warwick.ac.uk*
*lsalassa@cicbiomagune.es*

[b] *Dr. C. Garino*
*Department of Chemistry and NIS Centre of Excellence*
*University of Turin, via Pietro Giuria 7, 10125 Turin (Italy)*

[c] *Prof. J. C. Mareque-Rivas, Dr. A. Habtemariam*
*Ikerbasque, Basque Foundation for Science*
*48011 Bilbao (Spain)*

[d] *Dr. A. Habtemariam*
*Department of Chemistry, University of Warwick*
*Coventry CV4 7AL (UK)*

[e] *Dr. L. Salassa*
*Kimika Fakultatea, Euskal Herriko Unibertsitatea and*
*Donostia International Physics Center (DIPC) P.K.*
*1072 Donostia-San Sebastián, Euskadi (Spain)*

*Supporting information for this article is available on the WWW under http://dx.doi.org/10.1002/chem.201503991.*

light through multiphotonic processes.[21,22] Conveniently, UV/Vis photons emitted by UCNPs upon NIR-light excitation can promote photochemical reactions in metal complexes and potentially switch on their biological effects. Ford and co-workers showed that the NIR irradiation of UCNPs loaded with either the Roussin black salt anion or the photoactivated CO-releasing moiety (photoCORM) *trans*-[Mn(2,2′-bipyridine)$(PPh_3)_2(CO)_2$] results in the release of NO and CO, respectively.[13,14] Similarly, we have demonstrated that related upconversion nanosystems promoted the release of pyridine from a Ru–polypyridyl complex[16] and the generation of a $Pt^{II}$ species from a $Pt^{IV}$ prodrug candidate.[17] Alternatively, He et al. designed an UCNP system capable of releasing doxorubicin in a controlled fashion by taking advantage of a photoactivatable Ru complex that acts as a valve.[20] Conversely, Bonnet and co-workers also reported a promising system for activation at $\lambda = 630$ nm of a model Ru–polypyridyl complex by using triplet–triplet annihilation upconversion.[23]

The unique optical (upconversion emission) and chemical (e.g., $Gd^{3+}$ and $^{18}F^-$ ions on the surface) features of UCNPs are also exploited for multimodal imaging (i.e., single-photon emission computed tomography/positron emission tomography (SPECT/PET),[24,25] computed tomography (CT),[26] magnetic resonance imaging (MRI),[27] optical,[28] and photoacustic),[29] as demonstrated by numerous studies in vivo, which have appeared in the last few years. These properties and the low toxicity of UCNPs[30] make hybrid nanomaterials based on UCNPs and metal complexes suitable for application in theranostics.[31]

Herein, we devise a new approach to demonstrate the usefulness of UCNPs in the photoactivation of $Ru^{II}$–arene complexes, an attractive class of metal complex with remarkable anticancer activity in vitro[32,33] and in vivo.[34] Pyridinato $Ru^{II}$–arene derivatives display dark-stability and selectively release pyridinato ligands upon visible-light excitation, thus generating highly reactive aqua species.[35–37] Controlling such a reaction is key for activating the biological activity of $Ru^{II}$–arene derivatives.

For this purpose, we prepared two new Ru–pyridinato derivatives, namely $[(\eta^6\text{-}p\text{-cym})Ru(bpy)(m\text{-CCH-Py})][(PF_6)]_2$ (**1**) and $[(\eta^6\text{-}p\text{-cym})Ru(bpm)(m\text{-CCH-Py})][(PF_6)]_2$ (**2**; *p*-cym = *p*-cymene, bpy = 2,2′-bipyridine, bpm = 2,2′-bipyrimidine, and *m*-CCH-Py = 3-ethynylpyridine) and exploited a click-chemistry strategy to derivatise the monodentate 3-ethynylpyridine pendant arm with a phosphonate group, which has high affinity for the UCNP surface.[38] The functionalised complexes **3** and **4** and their precursors were characterised and their photochemistry studied in detail by using different methods, including DFT calculations.

On the basis of its photoreactivity, complex **4** was selected to anchor onto the core@shell $NaYF_4$:Yb(30%)/Tm(0.5%)@$NaYF_4$ nanoparticles and perform NIR photochemistry experiments. Results proved the obtained **UCNP@4** nanoconstruct is activated at $\lambda = 980$ nm, thus generating the reactive aqua photoproduct $[(\eta^6\text{-}p\text{-cym})Ru(bpm)(H_2O)]^{2+}$, which binds the DNA-model base guanosine 5′-monophosphate (GMP).

The synthetic strategy and NIR photoactivation reported herein may offer new intriguing opportunities for the design of innovative prodrug nanosystems that rely on the rich anticancer properties of metallo–arene complexes.

## Results and Discussion

### Synthesis of complexes 1–4 and UCNP@4

Complexes $[(\eta^6\text{-}p\text{-cym})Ru(bpy)(m\text{-CCH-Py})][(PF_6)]_2$ (**1**) and $[(\eta^6\text{-}p\text{-cym})Ru(bpm)(m\text{-CCH-Py})][(PF_6)]_2$ (**2**) were synthesised in moderate yields (ca. 35%) by treating the precursors $[(\eta^6\text{-}p\text{-cym})Ru(bpy)Cl][PF_6]$ and $[(\eta^6\text{-}p\text{-cym})Ru(bpm)Cl][PF_6]$ with $AgNO_3$ and subsequently performing ligand-exchange reactions with 3-ethynylpyridine in MeOH/$H_2O$ (Scheme 1 A).[39–42] A range of techniques was used to characterise both complexes, including X-ray, multinuclear NMR, mass-spectrometry, and elemental analysis.

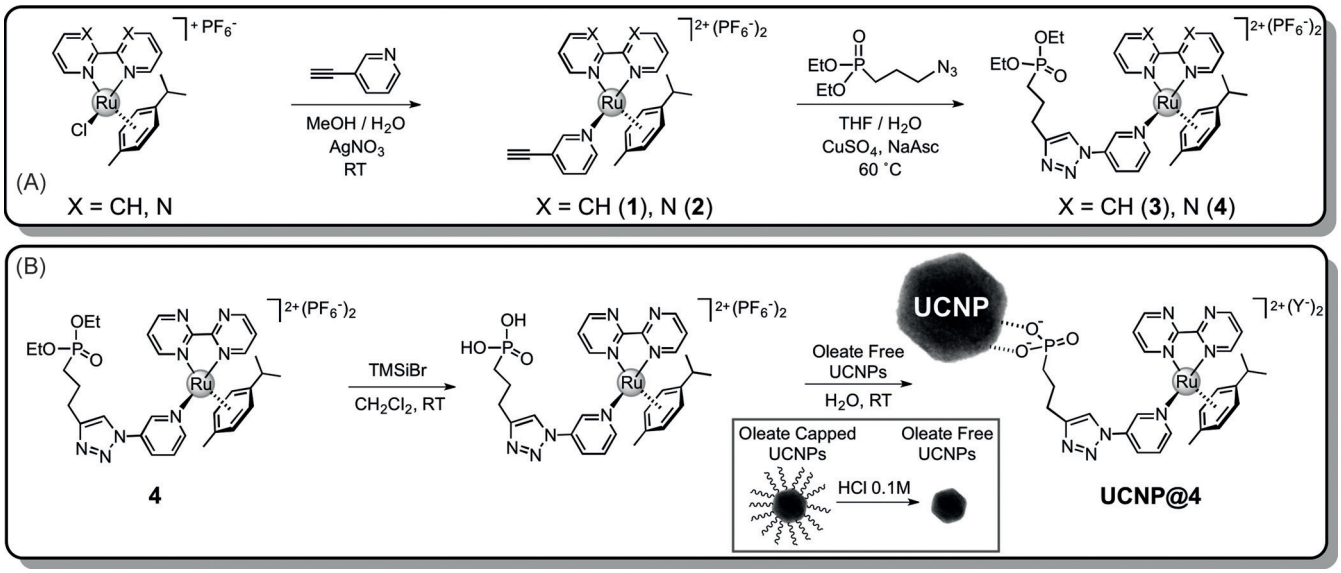


**Scheme 1.** Schematic representation of the approaches employed for the synthesis of A) **1**–**4** and B) **UCNP@4**. NaAsc = sodium ascorbate.

We employed 3-ethynylpyridine because pyridyl ligands are known to render Ru–arene complexes hydrolytically stable in the dark.[35–37] Moreover, the presence of an alkyne group on the ligand allowed us to adopt click chemistry for the functionalisation of **1** and **2** and anchoring onto UCNPs. Click chemistry is a convenient strategy for ligand design in inorganic chemistry and has attracted significant attention in recent years.[43] Such an approach affords (bio)orthogonal reactions that are high yielding, selective, and robust under mild conditions.[44]

Inspired by the work of Branda and co-workers,[45] we employed diethyl-3-azidopropyl phosphonate and its azido function to incorporate the phosphonate group into **1** and **2** by using click chemistry. Phosphonates have good affinity for the $NaYF_4$ surface of UCNPs and improve their biocompatibility, as demonstrated by various groups.[38,46]

Diethyl-3-azidopropyl phosphonate was obtained reacting (3-bromopropyl)phosphonic acid with sodium azide in acetone.[47] Clicked complexes $[(\eta^6\text{-p-cym})Ru(bpy)(P\text{-Trz-Py})][(PF_6)]_2$ (**3**) and $[(\eta^6\text{-p-cym})Ru(bpm)(P\text{-Trz-Py})][(PF_6)]_2$ (**4**; P-Trz-Py = [3-(1-pyridin-3-yl-[1,2,3]triazol-4-yl)-propyl]phosphonic acid diethyl ester) were prepared by treating **1** and **2** with diethyl-3-azidopropyl phosphonate in THF/water at 60 °C for 72 hours in the presence of $CuSO_4$ and sodium ascorbate (Scheme 1 A). Complexes **3** and **4** were obtained in good yields and purity and were characterised by $^1H$, $^{13}C$, and $^{31}P$ NMR spectroscopic and mass-spectrometric analysis.

Although the photochemical behaviour of the complexes is rather similar (see below), complex **4** was selected for loading onto the core@shell $NaYF_4$:$Yb^{3+}$/$Tm^{3+}$@$NaYF_4$ UCNPs on the basis of the higher reactivity of its bpm analogue **2** relative to **1** (i.e., with the bpy ligand). For this reason, we first activated the phosphonate group of **4** into the acid form by de-esterification with tribromo(methyl)silane (TMSBr) in $CH_2Cl_2$. The so-obtained complex was stirred overnight with oleate-free core@shell UCNPs in $H_2O$, and an orange pellet corresponding to **UCNP@4** was collected after several washing and centrifugation steps (Scheme 1 B). Characterisation of the hybrid material was achieved by using a combination of different techniques (see below).

## Characterisation and photochemical properties of 1 and 2

### *X-ray and DFT structures*

The crystal structure of the hexafluorophosphate salts of **1** and **2** were determined by means of X-ray diffraction studies (Figure 1). These structures are fairly similar, and the first-coordination spheres of both Ru complexes display comparable bond lengths and angles (Table 1). Complexes **1** and **2** present the typical piano-stool geometry of related $Ru^{II}$–arene complexes with N,N′ ancillary ligands.[41] Crystal packing and experimental details, including the X-ray diffraction data, are reported in the Supporting Information (see Table S1 and Figures S1 and S2 in the Supporting Information). DFT-optimised ground-state geometries (Table 1, B3LYP/LanL2DZ/6-31G**) for **1** and **2** describe the structure of the complexes satisfactorily. The calculated and experimental Ru–N bond lengths differ only by less than 0.02 Å. However, the Ru–*p-cym*(centroid) distances are approximately 0.15 Å longer in the DFT calculations relative to the X-ray determinations.

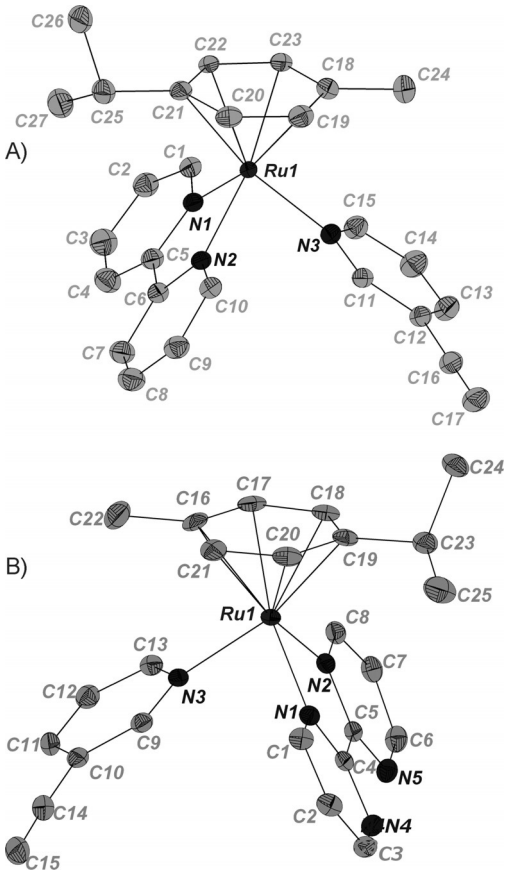


**Figure 1.** Crystal structures of A) **1** and B) **2**. Thermal ellipsoids are depicted at the 50% probability level. Counterions ($PF_6^-$) and hydrogen atoms have been omitted for clarity.

**Table 1.** Selected X-ray and DFT-calculated bond lengths [Å] for **1** and **2** in the ground-state (S0) and in two triplet-state (T0 and T1) geometries.

| Compd. | Ru–N(*m*-CCH-Py) | Ru–N(N,N′) | Ru–N(N,N′) | Ru–*p*-cym$_{(centroid)}$ |
|---|---|---|---|---|
| X-ray | | | | |
| 1 | 2.125(2) | 2.085(2) | 2.084(2) | 1.701 |
| 2 | 2.1241(17) | 2.0995(16) | 2.0873(16) | 1.704 |
| Ground state (S0) | | | | |
| 1 | 2.159 | 2.103 | 2.095 | 1.848 |
| 2 | 2.158 | 2.111 | 2.106 | 1.850 |
| Lowest-lying triplet state (T0) | | | | |
| 1 | 2.164 | 2.404 | 2.113 | 2.079 |
| 2 | 2.143 | 2.457 | 2.131 | 2.082 |
| Triplet state (T1) | | | | |
| 1 | 2.556 | 2.087 | 2.082 | 2.157 |
| 2 | 2.511 | 2.093 | 2.113 | 2.140 |

Two triplet excited-state structures were also DFT-minimised for **1** and **2** (Table 1) because triplet states are likely to be involved in the photochemistry of the complexes. The lowest-lying triplet state (T0) for both compounds has a distorted structure with one Ru–N(N,N′) bond strongly elongated (> 2.40 Å). However, the higher-energy triplet geometries (T1) for both compounds display elongated Ru–N(*m*-CCH-Py) distances (> 2.51 Å).

### *Photophysical and photochemical properties of 1 and 2*

The UV/Vis spectrum (see Figure S3 in the Supporting Information) of **1** exhibits five distinct bands at $\lambda = 245$, 269, 305, 317, and 370 nm ($\varepsilon = 7600$, 6400, 5400, 5700, and 1300 $M^{-1}cm^{-1}$, respectively), whereas **2** (Figure 2A) displays two major bands and one shoulder, respectively at $\lambda = 246$, 370, and 291 nm ($\varepsilon = 3700$, 1200, and 3200 $M^{-1}cm^{-1}$). Time dependent (TD)-DFT is a valuable tool to assign the character of the absorption bands. Calculation of singlet–singlet transitions and analysis of their orbital composition (see Tables S2 and S3 and Figure S4 in the Supporting Information) provide information on the nature of the singlet-excited states, which can be conveniently visualised by using electron-density difference maps (EDDMs; see Figures S5 and S6 in the Supporting Information).

In agreement with related complexes, the high-energy bands of **1** and **2** have mixed metal-to-ligand charge transfer (MLCT) and intraligand character (< 325 nm). Conversely the lowest-energy bands have mainly MLCT character. Furthermore, transitions of weak intensity with mixed MLCT/MC (metal-centred) character are present in their tail. These latter transitions have a significant contribution from σ-antibonding orbitals, which confer a dissociative nature (see Figure S4 in the Supporting Information). Through generation of these dissociative singlet states and subsequent intersystem crossing, the low-energy triplet states T0 and T1 (Figure 2B) can be populated. T1 is dissociative toward the 3-ethynylpyridine ligand, whereas T0 might promote the partial dissociation of a pyridyl ring of the bpy/bmp ligand (see Figures S7–S9 in the Supporting Information). Nevertheless, release of the chelating ligands is prevented by the strong coordination of the second ring. For this reason, light excitation of **1** and **2** results in selective photodissociation of the monodentate 3-ethynylpyridine ligand. Figure 2B reports the energy level of selected singlet and triplet states for **2** and their corresponding EDDMs (singlet states) and spin densities (triplet states; see Figure S10 for **1** in the Supporting Information).

The low energy of the T0 state (1.33 and 1.29 eV for **1** and **2**, respectively) calculated by DFT calculations and the small energy difference between this state and T1 are consistent with the lack of emission from the two complexes, which tend to relax to the ground state by nonradiative pathways, and

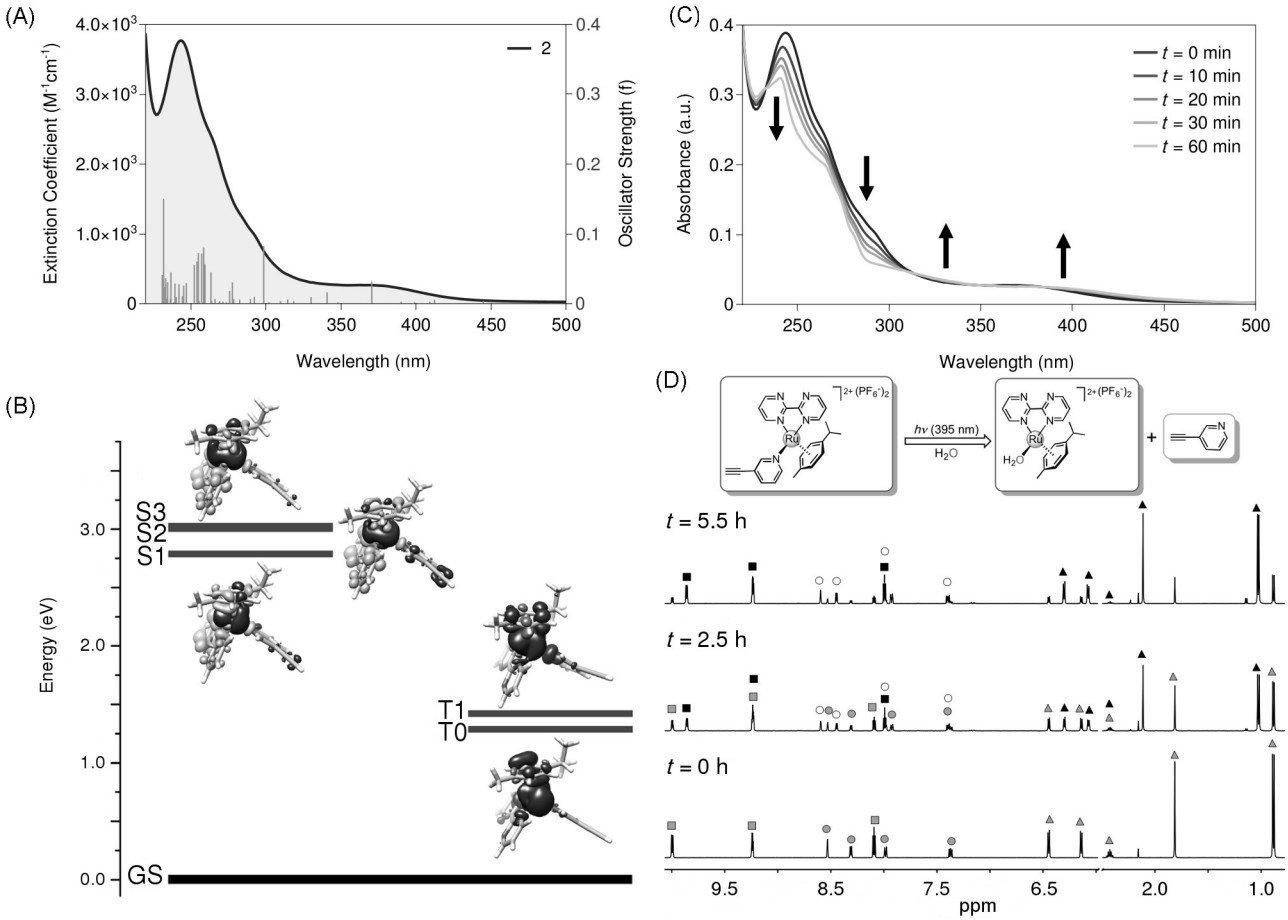


**Figure 2.** A) UV/Vis absorption spectrum of **2** in aqueous solution (95:5 = $H_2O$/DMSO); vertical bars represent singlet–singlet TD-DFT transitions (see Table S2 in the Supporting Information). B) Singlet and triplet energy-level diagram with EDDMs (singlets) and spin-density surfaces (triplet states) for **2**. In the EDDMs, black indicates a decrease in electron density, whereas gray indicates an increase. Time-course photolysis reactions for **2** in aqueous solution (95:5 = $D_2O$/[$D_6$]DMSO) upon $\lambda = 395$ nm excitation (15 mW $cm^{-2}$) followed by C) UV/Vis and D) $^1$H NMR spectroscopic analysis. $^1$H NMR: **2** (gray), [($\eta^6$-*p*-cym)Ru(bpm)($H_2O$)]$^{2+}$ (black), and free 3-ethynylpyridine (white); ■ = bpm, ▲ = *p*-cym, ● = 3-ethynylpyridine.

with their modest photodissociation quantum yields of less than 1%, as determined by using actinometry methods[48] ($\Phi_1 = 0.003$ and $\Phi_2 = 0.008$; see Table S4 and Figures S11–S14 in the Supporting Information).

Figure 2C,D shows the photolysis of **2** ($D_2O$/[$D_6$]DMSO, 95:5%) upon light irradiation at $\lambda = 395$ nm (15 mW cm$^{-2}$) followed by UV/Vis and $^1$H NMR spectroscopic analysis. Light irradiation induces variations in the UV/Vis absorption profile of **2**, with a decrease at $\lambda = 370$ nm and an increase at $\lambda = 260$–320 nm of the bands. The presence of isosbestic points at $\lambda =$ 230 and 315 nm reveals the formation of a single photoproduct.

Furthermore, diagnostic changes in the $^1$H NMR spectra of **2** and ultraperformance (UP) LC-MS analysis (see Figure S15 in the Supporting Information) clearly confirm the release of 3-ethynylpyridine and the formation of the aqua [($\eta^6$-*p*-cym)Ru(bpm)($H_2O$)]$^{2+}$ ionic species.[35–37] A control experiment indicates **2** is stable in the dark up to at least 24 hours (see Figure S16 in the Supporting Information). Analogue results were observed for **1** and are summarised in Figures S17–S19 (see the Supporting Information).

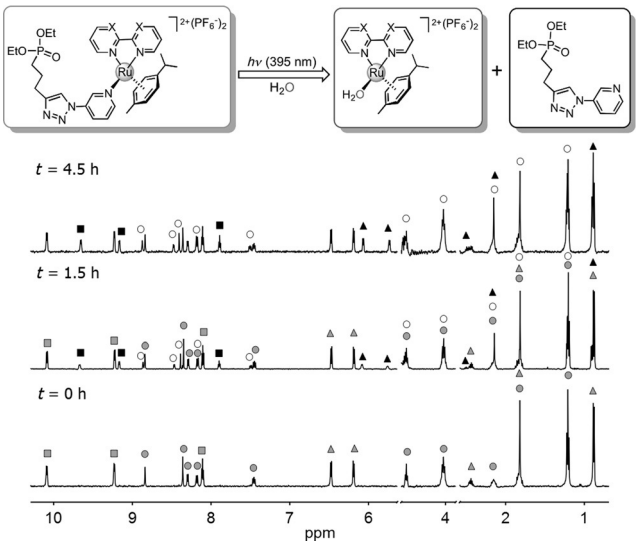


**Figure 3.** Photolysis time course for **4** in aqueous solution (95:5 = $H_2O$/[$D_6$]DMSO) upon $\lambda = 395$ nm excitation (15 mW cm$^{-2}$) followed by $^1$H NMR spectroscopic analysis. $^1$H NMR: **4** (gray), [($\eta^6$-*p*-cym)Ru(bpm)($H_2O$)]$^{2+}$ (black), and free P-Trz-Py (white); ■ = bpm, ▲ = *p*-cym, ● = P-Trz-Py.

## NIR photochemistry with UCNPs

### *Photochemistry of 3, 4, and UCNP@4 under visible- and NIR-light excitation*

Initially, the behaviour of clicked complexes **3** and **4** was verified and compared with their analogues **1** and **2** in the dark and under visible-light conditions. Analysis by NMR spectroscopy and UPLC-MS (see Figure 3 and Figures S20–S23 in the Supporting Information) shows that **3** and **4** indeed react as the precursors **1** and **2**; namely, **3** and **4** undergo photodissociation of the P-Trz-Py ligand upon excitation at $\lambda = 395$ nm. The addition of excess GMP to irradiated solutions of **3** and **4** results in the formation of the adducts [($\eta^6$-*p*-cym)Ru(bpy)(GMP)]$^{2+}$ and [($\eta^6$-*p*-cym)Ru(bpm)(GMP)]$^{2+}$ after 12 hours of incubation at ambient temperature (see Figures S24–S27 in the Supporting Information). Next, we selected **4** to perform decoration of UCNPs because of the slightly higher photodissociation yield of bpm complexes with respect to their bpy analogues.

For anchoring of **4** to UCNPs, we first synthesised core@shell $NaYF_4$:$Yb^{3+}$/$Tm^{3+}$(30/0.5%)@$NaYF_4$ nanoparticles by thermal decomposition as previously described by several groups (see the Experimental Section and the Supporting Information).[17,49,50] UCNPs were thoroughly characterised by TEM, X-ray photospectroscopy (XPS), and FTIR and emission spectroscopy (see Figures S28–S32 in the Supporting Information). TEM images of the core@shell UCNPs show uniform size and shape (diameter = 37 nm; Figure 4A).

Functionalisation with **4** was achieved as described in Scheme 1B and did not cause any observable change to the nanoparticles, rather TEM images of aqueous solutions of **UCNP@4** showed improved dispersion and lower aggregation relative to the core-only and core@shell UCNPs capped with oleic acid. We obtained a rough estimate of the complex-grafting density onto UCNPs by UV/Vis spectroscopic analysis following the procedure of Branda and co-workers.[51] By assuming a particle density of 4.2 g cm$^{-3}$ and a diameter of 36.9 nm, the **4**/UCNP ratio was calculated to be approximately 3000:1 (3.5% wt). The UCNPs display a typical upconversion emission in THF of $Tm^{3+}$ ions (Figure 4) with peaks at $\lambda = 345$ and 360 nm ($^3P_0 \rightarrow {}^3F_4$ and $^1D_2 \rightarrow {}^3H_6$); $\lambda = 450$ and 475 nm ($^1D_2 \rightarrow {}^3F_4$ and $^1G_4 \rightarrow {}^3H_6$); $\lambda = 645$, 690, and 720 nm ($^1G_4 \rightarrow {}^3F_4$ and $^3F_3 \rightarrow {}^3H_6$), and at $\lambda = 800$ nm ($^3H_4 \rightarrow {}^3H_6$). Photoluminescence studies confirm that core@shell NPs present more intense emissions relative to their core counterparts, especially in the blue region of the UV spectrum (see Figure S32 in the Supporting Information). The undoped $NaYF_4$ shell is essential to improve the efficiency of the upconversion process as it decreases nonradiative decay due to the solvent and capping ligands.[49]

As we demonstrated previously,[17] such an improvement is key to take full advantage of the overlap between the emission spectrum of UCNPs and the absorption spectrum of metal complexes (Figure 4B). No significant changes in UCNP luminescence was detected once the particles were treated with hydrochloric acid to remove the oleic acid, thus favouring the interaction with the phosphonic acid group of (activated) **4**. Surface modification was confirmed first by the colour of the UCNPs, which became pale orange, and then by UV/Vis spectroscopic analysis of **UCNP@4** suspended in aqueous solution and by XPS. The UV/Vis spectrum of **UCNP@4** (Figure 4B) exhibits the absorption profile of the complex with bands at $\lambda =$ 261 and 370 nm. Notably, the spectrum shows the characteristic band of the dopant $Yb^{3+}$ ion at $\lambda = 980$ nm.

Aqueous solutions of **4** and **UCNP@4** were deposited onto titanium supports for XPS measurements (see Figure 4C,D and Figures S33 and S34 in the Supporting Information). The expected Ru and P peaks for the $Ru^{2+}$ ion and the phosphonic group of the ligand, respectively, were observed in both samples; however, a dramatic difference appeared in the P $2p_{3/2}$

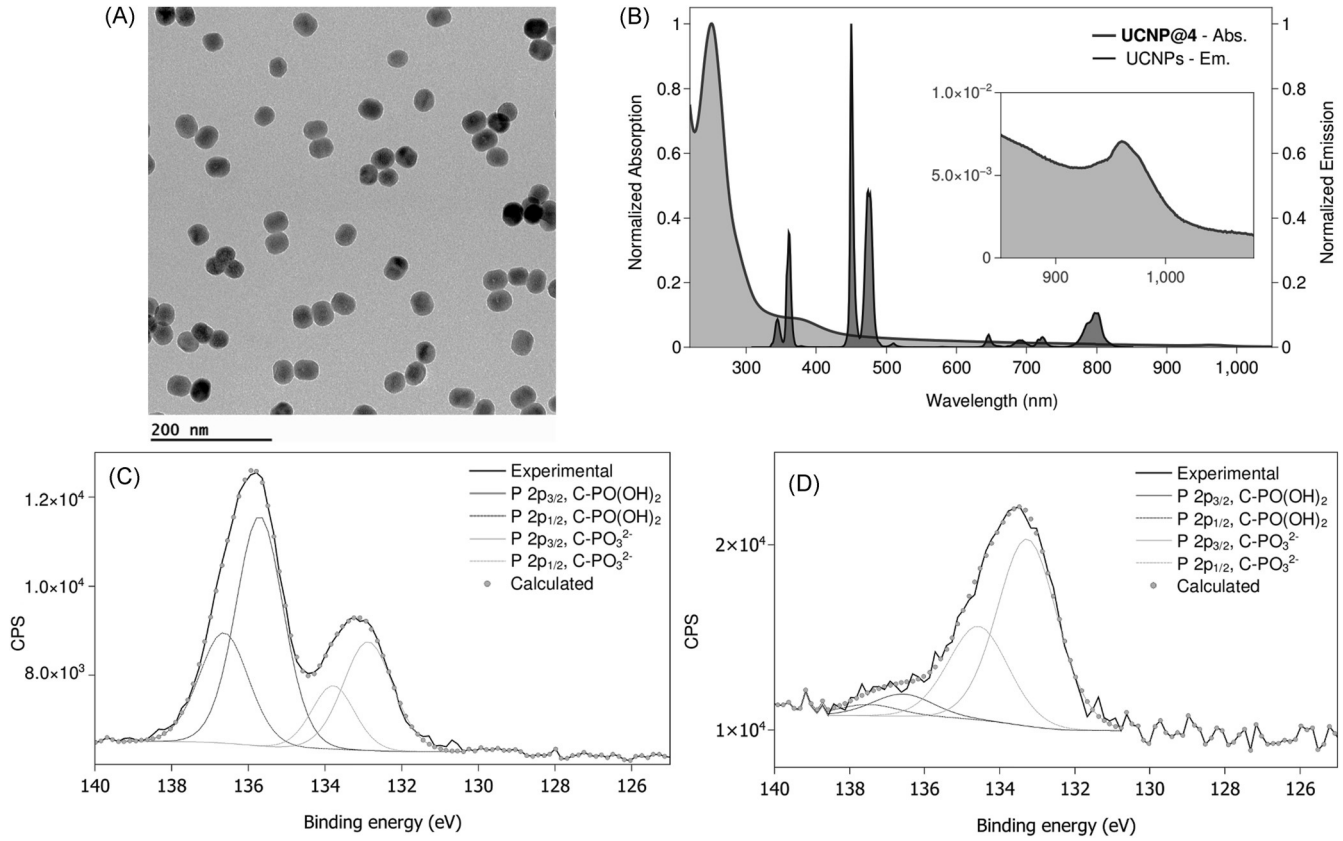


**Figure 4.** A) TEM image of **UCNP@4**. B) Overlap between the normalised absorption (gray) and emission (dark gray) spectrum of **UCNP@4** of core@shell UCNPs (THF) upon excitation at $\lambda = 980$ nm (15 W cm$^{-2}$). Inset: enlargement of the region $\lambda = 900$–1000 nm for the absorption of **UCNP@4** in aqueous solution. P $2p_{3/2}$, $2p_{1/2}$ XPS spectra of C) **4** and D) **UCNP@4**.

and $2p_{1/2}$ region. In particular, the protonation state of the phosphonic group was clearly different in the case of **UCNP@4** relative to **4**. The former showed a much greater proportion of R–$PO_3^{2-}$ versus R–$PO(OH)_2$ groups (90:10 and 33:67 for **UCNP@4** and **4**, respectively) in agreement with the formation of electrostatic interactions between the phosphonic group of the complex and the surface of the UCNPs.

Therefore, we investigated the effects of NIR light on **UCNP@4** in aqueous solution by irradiating at $\lambda = 980$ nm and monitoring the course of photoreaction by $^1$H NMR spectroscopic analysis, which was possible despite the decreased resolution of the $^1$H NMR spectrum of **UCNP@4** due to the intrinsic paramagnetism of UCNPs.

Remarkably, the NMR spectra of the NIR-irradiated **UCNP@4** display changes in the signal pattern (Figure 5), thus resembling the spectra observed for **4** under excitation at $\lambda =$ 395 nm and ultimately confirming the formation of the $[(\eta^6\text{-}p\text{-cym})Ru(bpm)(H_2O)]^{2+}$ ion. Moreover, UPLC-MS experiments consistently show an optimal agreement in retention time and *m/z* values for irradiated solutions of **4** and **UCNP@4** (at $\lambda =$ 395 and 980 nm; see Figures S21 and S35 in the Supporting Information).

The aqua photoproduct generated by NIR light at the UCNP surface reacts with GMP to afford the adduct $[(\eta^6\text{-}p\text{-cym})Ru(bpm)(GMP)]^{2+}$ (as confirmed by using NMR spectroscopy and UPLC-MS; see Figures S36 and S37 in the Supporting Information), hence demonstrating that the reactivity of $Ru^{II}$ complexes toward biological targets can be triggered by low-energy photons.

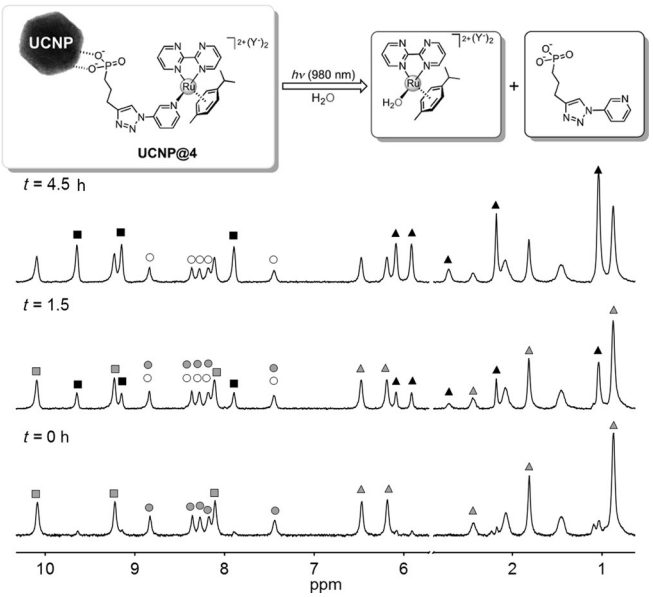


**Figure 5.** Photolysis time course for **UCNP@4** in aqueous solution upon excitation at $\lambda = 980$ nm (8.1 W cm$^{-2}$) followed by $^1$H NMR spectroscopic analysis. $^1$H NMR: **UCNP@4** (gray), P-Trz-Py (black), and $[(\eta^6\text{-}p\text{-cym})Ru(bpm)(H_2O)]^{2+}$ (white); ■ = bpm, ▲ = *p*-cym, ● = P-Trz-Py.

Control experiments indicate that **UCNP@4** is stable and does not undergo ligand dissociation in the dark, whereas **4** (and **2**) does not photoreact when irradiated by NIR light for several hours (see Figures S38 and S39 in the Supporting Information).

The photochemical efficiency of these hybrid systems still needs to be improved for more advanced applications; however, the combination of UCNP optical features with their multimodal-imaging capability can open new intriguing opportunities for innovative application in theranostics.

## Conclusion

Herein, we have reported the synthesis of two new photoactivatable Ru–arene complexes **1** and **2** and the thorough characterisation of their structural and photochemical proprieties. In addition, we have demonstrated that click chemistry is a valuable strategy to introduce a phosphonate group directly on complexes **1** and **2** by exploiting the alkyne function on the 3-ethynylpyridyl ligand coordinated to their Ru centres. As in the case of their precursors, the so-obtained derivatives **3** and **4** selectively release the pyridyl ligand under direct light excitation of their lowest-energy absorption band. Moreover, phosphonate groups on **3** and **4** confer these complexes high affinity for the surface of core@shell $NaYF_4$:Yb/Tm@$NaYF_4$ upconverting nanoparticles.

Notably, ligand photodissociation and GMP coordination is triggered under excitation at $\lambda = 980$ nm when **4** is anchored on UCNPs (**UCNP@4**), thus providing, to the best our knowledge, the first example of remote near-infrared photoactivation of a $Ru^{II}$–arene model prodrug.

Although UCNPs have been intensively investigated for medical applications, research into their combination with coordination compounds is still very limited. The approach that we proposed herein is of general applicability in terms of synthetic and photoactivation strategies. The 3-ethynylpyridyl ligand is indeed a convenient candidate on which to perform click chemistry reactions in the proximity of transition-metal centres. Furthermore, the aliphatic arm of the azido-phosphonate ligand can be opportunely changed to modify the distance between the UCNPs and photoactivatable complexes and perhaps modulate their photochemistry.

Our proof of concept study demonstrates that UCNPs are convenient platforms for the use of deep-penetrating NIR light in the activation of anticancer metal complexes and the generation of active species in situ.

## Experimental Section

### Materials

$RuCl_3 \cdot 3H_2O$ (99%) was purchased from Precious Metals Online (PMO Pty Ltd) and used as received. 2,2′-Bipyrimidine (bpm; 97%), 2,2′-bipyridine (bpy; ≥99%), silver nitrate ($AgNO_3$; ≥99%), potassium hexafluorophosphate ($KPF_6$; 98%), 3-ethynylpyridine (98%), yttrium(III) acetate hydrate (99.9%), ytterbium(III) acetate tetrahydrate (99.9%), thulium(III) acetate hydrate (99.9%), 1-octadecene (technical grade, 90%), oleic acid (technical grade, 90%), sodium hydroxide (≥97%), ammonium fluoride (98%), iron(III) chloride (97%), potassium oxalate monohydrate (99%), sodium azide (≥95%), guanosine 5′-monophosphate disodium salt hydrate (≥99%), and all the solvents were obtained from Sigma–Aldrich and were used as received.

### Synthesis of ruthenium complexes

The dimer $[\{(\eta^6\text{-}p\text{-cym})RuCl_2\}_2]$ and the $Ru^{II}$ complexes $[(\eta^6\text{-}p\text{-cym})Ru(bpy)Cl][PF_6]$ and $[(\eta^6\text{-}p\text{-cym})Ru(bpm)Cl][PF_6]$ were prepared based on previous reports.[39–41] The $Ru^{II}$–pyridinato complexes **1**–**4** were prepared based on a previously reported methodology with some modifications.[42]

**$[(\eta^6\text{-}p\text{-cym})Ru(bpy)(m\text{-CCH-Py})][(PF)_6]_2$ (1)**: $AgNO_3$ (0.2 g, 1.175 mmol) was added to an aluminium-foil-covered round-bottom flask charged with $[(\eta^6\text{-}p\text{-cym})Ru(bpy)Cl][PF_6]$ (500 mg, 1.2 mmol) in a 1:1 mixture of MeOH/$H_2O$ (50 mL). The reaction mixture was stirred at ambient temperature for 18 h. The solution turned light yellow, and the off-white AgCl precipitate was filtered off. 3-Ethynylpyridine (620 mg, 6 mmol) was added to the clear yellow solution of $[(\eta^6\text{-}p\text{-cym})Ru(bpy)(H_2O)]^{2+}$ to give a dark-red solution. The reaction mixture was heated at 40 °C for 18 h, and $KPF_6$ (1.3 g, 7.2 mmol) was added after cooling. The precipitate that formed was dissolved by the addition of acetone to give a clear solution, which was filtered. The solution was reduced in volume until the onset of precipitation on the rotary evaporator and left to evaporate slowly at ambient temperature to afford yellowish flakes, which were collected by filtration, washed with methanol and diethyl ether, and dried in air (330 mg, 35%). $^1$H NMR (500 MHz, $D_2O$): $\delta = 0.82$ (d, $^3J(H,H) = 6.9$ Hz, 6H), 1.77 (s, 3H), 2.41 (spt, $^3J(H,H) = 7.0$ Hz, 1H), 5.99 (d, $^3J(H,H) = 6.4$ Hz, 2H), 6.40 (d, $^3J(H,H) = 6.5$ Hz, 2H), 7.30 (dd, $^3J(H,H) = 8.0$, 5.9 Hz, 1H), 7.86 (td, $^3J(H,H) = 7.3$, 5.7, 2H), 7.93 (dt, $^3J(H,H) = 8.1$, 1.5 Hz, 1H), 8.22 (td, $^3J(H,H) = 7.9$, 1.4 Hz, 2H), 8.30 (m, 3H), 8.51 (s, 1H), 9.64 ppm (d, $^3J(H,H) = 5.0$ Hz, 2H); the proton resonance of the alkyne group overlaps with residual water signal in $D_2O$, whereas this proton resonates at $\delta = 4.73$ ppm (s, 1H) in [D$_6$]DMSO; $^{13}$C NMR (125 MHz, [D$_6$]DMSO): $\delta = 17.9$, 22.2, 30.6, 78.5, 84.9, 87.5, 92.5, 103.7, 108.8, 122.0, 125.1, 127.1, 129.5, 141.8, 143.3, 152.8, 155.1, 155.4, 156.7 ppm; FTIR (KBr pellet) $\tilde{\nu}_{max} = 3300$, 1580, 1410, 840, 560 cm$^{-1}$; ESI-MS: *m/z* ($H_2O$/MeOH) calcd for $[C_{27}H_{27}N_3RuPF_6]^+$: 640.09; found: 640.30; elemental analysis calcd (%) for $C_{27}H_{27}F_{12}N_3P_2Ru$: C 41.34, H 3.47, N 5.36; found: C 40.94, H 3.12, N 5.08.

**$[(\eta^6\text{-}p\text{-cym})Ru(bpm)(m\text{-CCH-Py})][(PF)_6]_2$ (2)**: Complex **2** was synthesised by using the procedure described for **1** with the $[(\eta^6\text{-}p\text{-cym})Ru(bpm)Cl][PF_6]$ precursor (200 mg, 0.48 mmol). Yield: (120 mg, 32%); $^1$H NMR (500 MHz, $D_2O$): $\delta = 0.88$ (d, $^3J(H,H) = 6.9$ Hz, 6H), 1.81 (s, 3H), 2.43 (spt, $^3J(H,H) = 7.0$ Hz, 1H), 6.14 (d, $^3J(H,H) = 6.5$ Hz, 2H), 6.44 (d, $^3J(H,H) = 6.5$ Hz, 2H), 7.37 (dd, $^3J(H,H) = 8.0$, 5.8 Hz, 1H), 7.98 (dt, $^3J(H,H) = 8.0$, 1.5 Hz, 1H), 8.09 (dd, $^3J(H,H) = 5.8$, 4.9 Hz, 2H), 8.31 (d, $^3J(H,H) = 5.8$ Hz, 1H), 8.53 (s, 1H), 9.24 (dd, $^3J(H,H) = 4.8$, 1.9 Hz, 2H), 10.00 ppm (dd, $^3J(H,H) = 5.8$, 1.9 Hz, 2H); the proton of the alkyne group overlaps the residual water signal in $D_2O$, whereas this proton resonates at $\delta = 4.72$ ppm (s, 1H) in [D$_6$]DMSO; $^{13}$C NMR (125 MHz, [D$_6$]DMSO): $\delta = 17.7$, 22.2, 30.4, 78.8, 86.1, 87.3, 90.8, 106.3, 107.6, 122.0, 126.0, 126.9, 143.0, 153.4, 156.0, 160.8, 161.5, 164.1 ppm; FTIR (KBr pellet) $\tilde{\nu}_{max} = 3300$, 1580, 1410, 840, 560 cm$^{-1}$; ESI-MS: *m/z* ($H_2O$/MeOH) calcd for $[C_{25}H_{25}N_5RuPF_6]^+$: 642.08; found: 642.28; elemental analysis calcd (%) for $C_{25}H_{25}F_{12}N_5P_2Ru$: C 38.18, H 3.20, N 8.90; found: C 37.59, H 3.04, N 8.71.

**Diethyl-3-azidopropyl phosphonate**: The preparation of the azido ligand for click chemistry is based on the procedure reported by

Tucker-Schwartz and Garrell.[47] (3-Bromopropyl)phosphonic acid diethyl ether (5 mL, 26.02 mmol) was dissolved in acetone (25 mL) and dried by passing through neutral alumina. $NaN_3$ (2.6 g, 40.4 mmol) was added to the reaction mixture, which was heated to reflux for 18 h. The reaction mixture was cooled, filtered through celite, and washed several times with acetone. The solvent was removed by rotary evaporation to leave a clear yellowish oil (5.81 g, quantitative yield). $^1$H NMR (500 MHz, [D$_6$]DMSO): $\delta = 1.24$ (t, $^3J$(H,H) = 7.1 Hz, 6H), 1.78 (m, 4H), 3.41 (t, $^3J$(H,H) = 6.6 Hz, 2H), 4.00 ppm (m, 4H); $^{31}$P NMR (200 MHz, [D$_6$]DMSO): $\delta = 30.9$ ppm; FTIR (KBr pellet) $\tilde{\nu}_{max} = 3400, 3000, 2100, 1240, 1050, 960$ cm$^{-1}$.

**[($\eta^6$-p-cym)Ru(bpy)(P-Trz-Py)][(PF$_6$)$_2$]$_2$ (3)**: $CuSO_4$ (8 mg, 0.032 mmol), sodium ascorbate (6.3 mg, 0.032 mmol), and diethyl-3-azidopropyl phosphonate (14.4 mg, 0.064 mmol) were added to a solution of [($\eta^6$-p-cym)Ru(bpy)(*m*-CCH-Py)][(PF$_6$)$_2$]$_2$ (**1**; 50 mg, 0.064 mmol) in THF/$H_2O$ (4:1, 5 mL). The reaction mixture was heated at 60 °C for 72 h. $KF_6$ (9.5 g, 52 mmol) in $H_2O$ (30 mL) was then added to the reaction mixture, which was placed in a separating funnel and extracted with dichloromethane (3×10 mL) to give a reddish solution. This mixture was dried over $MgSO_4$, and the solvent was removed by rotary evaporation to give an oily product, which was dissolved in methanol. $KPF_6$ (2 g) was added to the solution and the product was precipitated by the addition of diethyl ether. The solid was collected by decanting the diethyl ether, the residue was redissolved in dichloromethane, and the precipitated salt was filtered off to obtain a red solid, which was dried in air (25 mg, 41%). $^1$H NMR (500 MHz, $D_2O$): $\delta = 0.83$ (d, $^3J$(H,H) = 6.9 Hz, 6H), 1.19 (t, $^3J$(H,H) = 7.1 Hz, 6H), 1.82 (m, 5H), 2.15 (m, 2H), 2.44 (stp, $^3J$(H,H) = 6.8 Hz, 1H), 4.02 (m, 4H), 4.49 (t, $^3J$(H,H) = 6.7 Hz, 2H), 6.05 (d, $^3J$(H,H) = 6.3 Hz, 2H), 6.44 (d, $^3J$(H,H) = 6.3 Hz, 2H), 7.40 (dd, $^3J$(H,H) = 8.1, 5.8 Hz, 1H), 7.89 (t, $^3J$(H,H) = 7.2 Hz, 2H), 8.14 (d, $^3J$(H,H) = 8.0 Hz, 1H), 8.22 (t, $^3J$(H,H) = 7.9 Hz, 2H), 8.29 (m, 4H), 8.79 (s, 1H), 9.72 ppm (d, $^3J$(H,H) = 6.0 Hz, 2H); $^{13}$C NMR (125 MHz, [D$_6$]DMSO): $\delta = 16.7, 17.9, 21.5, 22.2, 23.8, 30.6, 50.2, 61.6, 85.0, 92.3, 104.0, 108.6, 124.0, 125.1, 127.6, 129.5, 130.0, 136.8, 141.7, 141.8, 148.5, 152.4, 155.3, 156.7$ ppm; $^{31}$P NMR (200 MHz, [D$_6$]DMSO): $\delta = 30.4$ ppm; ESI-MS *m/z* ($H_2O$/MeOH) calcd for [$C_{34}H_{43}O_3N_6PRuPF_6$]$^+$: 861.18; found: 861.45.

**[($\eta^6$-p-cym)Ru(bpm)(P-Trz-Py)] [(PF$_6$)$_2$]$_2$ (4)**: Complex **4** was synthesised by using the procedure described above for **3** and starting from [($\eta^6$-p-cym)Ru(bpm)(*m*-CCH-Py)][(PF$_6$)$_2$]$_2$ (50 mg, 0.06 mmol). Yield: 15 mg, 23%; $^1$H NMR (500 MHz, $D_2O$): $\delta = 0.89$ (d, $^3J$(H,H) = 6.9 Hz, 6H), 1.21 (t, $^3J$(H,H) = 7.1 Hz, 6H), 1.82 (m, 5H), 2.16 (m, 2H), 2.45 (stp, $^3J$(H,H) = 6.8 Hz, 1H), 4.03 (m, 4H), 4.50 (t, $^3J$(H,H) = 6.8 Hz, 2H), 6.19 (d, $^3J$(H,H) = 6.4 Hz, 2H), 6.48 (d, $^3J$(H,H) = 6.4 Hz, 2H), 7.46 (dd, $^3J$(H,H) = 8.1, 5.8 Hz, 1H), 8.11 (dd, $^3J$(H,H) = 5.9, 4.8 Hz, 2H), 8.18 (dt, $^3J$(H,H) = 8.1, 1.6 Hz, 1H), 8.30 (d, $^3J$(H,H) = 5.7 Hz, 1H), 8.36 (s, 1H), 8.84 (s, 1H), 9.23 (dd, $^3J$(H,H) = 4.9, 1.9 Hz, 2H), 10.09 ppm (dd, $^3J$(H,H) = 5.9, 1.9 Hz, 2H); $^{13}$C NMR (125 MHz, [D$_6$]DMSO,) $\delta = 16.7, 17.8, 22.2, 22.7, 23.8, 30.5, 50.3, 61.6, 86.2, 90.6, 106.7, 107.5, 124.0, 126.0, 127.5, 130.1, 137.6, 142.0, 149.5, 152.9, 160.8, 161.5, 164.1$ ppm; $^{31}$P NMR (200 MHz, [D$_6$]DMSO): $\delta = 30.4$ ppm. ESI-MS *m/z* ($H_2O$/MeOH), calcd for [$C_{32}H_{41}O_3N_8PRuPF_6$]$^+$: 863.17; found: 863.42.

## Synthesis of UCNPS

The core@shell $NaYF_4$:Yb(30%)/Tm(0.5%)@$NaYF_4$ nanoparticles were synthesised in two steps by thermal decomposition, as previously reported by us[16] and others.[45,46] The oleate-coated core $NaYF_4$:$Yb^{3+}$/$Tm^{3+}$ (30/0.5%) nanoparticles were first synthesised by employing the acetate salts of Rare Earth elements (i.e., Y, Yb, and Tm) in solutions of oleic acid and octadecene. Subsequently, an undoped $NaYF_4$ protective shell was grown around on the surfaces of the core NPs by using the same synthetic procedure. Full synthetic details and characterisation (IR, XPS, TEM, optical proprieties) of the nanoparticles are reported in the Supporting Information.

## Synthesis of the adduct UCNP@4

Both **3** and **4** selectively photodissociate the P-Trz-Py ligand upon irradiation at $\lambda = 400$ nm. However, **4** was selected for the functionalisation of UCNPs (Scheme 1B) and NIR photolysis studies because the bpm derivative **2** displayed a slightly higher photodissociation yield relative to the bpy derivative **1**.

**Deprotection of [($\eta^6$-p-cym)Ru(bpm)(P-Trz-Py)][(PF$_6$)$_2$]$_2$ (4)**: We followed a similar procedure to that reported for the deprotection of diethyl-3-azidopropyl phosphonate to yield 3-azido propyl phosphoric acid.[47] An aluminium-foil-covered round-bottom flask was charged with [($\eta^6$-*p*-cym)Ru(bpm)(P-Trz-Py)][(PF$_6$)$_2$]$_2$ (**4**; 2.5 mg) in $CH_2Cl_2$ (anhydrous; 1 mL) to obtain a yellow solution. Trimethylsilyl bromide (TMSBr) was added (c.a. 10 drops) to the flask. Instantaneously, the reaction solution changed from transparent to cloudy. After the end of the addition, the reaction mixture was stirred overnight at ambient temperature. Afterward, the solvent was removed under gentle nitrogen flow to give a yellow precipitate.

**Preparation of oleate-free UCNPs**: The preparation was performed following a reported procedure by Bogdan et al.[52] The core@shell $NaYF_4$:Yb(30%)/Tm(0.5%)@$NaYF_4$ nanoparticles (50 mg) were suspended in $H_2O$ (5 mL) in a round-bottom flask. The mixture was adjusted to pH 4 by using 0.1 M HCl solution, and the suspension was stirred for 2 h at ambient temperature. Afterward, the oleate-free UCNPs were purified from the released oleic acid by extraction with diethyl ether (3×5 mL). The product (ca. 30 mg) was dried at ambient temperature overnight.

**Functionalisation of oleate-free UCNPs with 4**: Deprotected complex **4** (2.5 mg) was mixed with oleate-free core@shell $NaYF_4$:Yb/Tm@$NaYF_4$ (10 mg) and suspended in $H_2O$ (1.5 mL) in an aluminium-foil-covered round-bottom flask. The suspension was stirred overnight at ambient temperature and then freeze-dried. The obtained yellow powder was washed several times with ethanol and precipitated by centrifugation (10000 rpm for 5 min) to remove excess Ru complex. **UCNP@4** (ca. 6 mg) was dried at ambient temperature overnight. $^1$H NMR (500 MHz, $D_2O$): $\delta = 0.87$ (6H), 1.81 (3H), 2.16 (2H), 2.43 (1H), 4.47 (2H), 6.18 (2H), 6.47 (2H), 7.44 (1H), 8.11 (2H), 8.18 (1H), 8.27 (1H), 8.36 (1H), 8.83 (1H), 9.22 (2H), 10.09 ppm (2H). Note: All the proton signals of **UCNP@4** were broader than those of **4**, loss of multiplicity is due to the paramagnetic nature of the UCNPs, and four aliphatic protons relative to the propyl chain of the phosphonic acid group gave signals too broad to be observed (previously falling in at $\delta_H = 4.03$ ppm in **4**) due to their proximity to the surface of UCNPs.

## Photolysis experiments

**Photoirradiation of Ru complexes at $\lambda = 395$ nm**: Aqueous solutions of **1**–**4** were irradiated at $\lambda = 395$ nm on a Prizmatix LED Multiwavelength MWLLS-11 source (15 mW cm$^{-2}$) at ambient temperature. The progress of the photoreaction was followed by using $^1$H NMR or UV/Vis spectroscopy. Finally, the nature of the photoproducts was also analysed by UPLC-MS.

**Photoirradiation of 4 and UCNP@4 at $\lambda = 980$ nm**: Aqueous solutions of **4** and **UCNP@4** were irradiated at $\lambda = 980$ nm with a BWT diode laser DS3-11312-110. Complex **4** (150 μM, 400 μL) and **UCNP@4** (10 mg mL$^{-1}$, 400 μL) solutions were irradiated for 7 and 5.5 h (8.8 and 8.1 W cm$^{-2}$, respectively). The progress of the photo-

reaction was followed by $^{1}H$ NMR spectroscopic measurements, after solutions of **UCNP@4** had been centrifuged (6000 rpm, 5 min) to improve the quality of the NMR spectra. The nature of the photoproducts was also analysed by UPLC-MS. The output-power density of the light sources employed was measured with an optical power meter (Ophir Photonics PD300-3W).

### NMR spectroscopy

$^{1}H$, $^{13}C$, and $^{31}P$ NMR spectra of the various samples in deuterated solvents ($D_2O$ or [$D_6$]DMSO) were acquired by using standard pulse programs on an Avance III Bruker 500 NMR spectrometer. The chemical shifts were reported in parts per million ($\delta$, ppm) and referenced to the residual solvent peak.

### X-ray crystallography

Diffraction data for **1** and **2** were obtained on an Agilent Super Nova Mo diffractometer coupled to a CCD area detector at 100 K using an Agilent 700 Cryosystem Cooler fed with liquid nitrogen. Full-matrix least-squares refinements based on *F*2 were performed by using SHELXL-97, and the structures were solved by direct methods. The rest of the hydrogen atoms were located by using a riding model. The crystallographic details of **1** and **2** have been deposited in the Cambridge Crystallographic Data Centre. CCDC 1055609 and 1055610 contain the supplementary crystallographic data for this paper. These data can be obtained free of charge from .

### FTIR spectroscopy

FTIR spectra of **1**, **2**, and core-$NaYF_4$:Yb/Tm, core@shell-$NaYF_4$:Yb/Tm@$NaYF_4$, and oleate-freecore@shell-$NaYF_4$:Yb/Tm@$NaYF_4$ nanoparticles were recorded on a Nicolet FTIR 6700 spectrometer as KBr disks.

### UV/Vis absorption spectroscopy

UV/Vis spectroscopic experiments of the Ru complexes and **UCNP@4** were performed in $H_2O$ on a Varian Cary 5000 spectrophotometer.

### Emission spectroscopy

The emission spectra of UCNP dispersions in THF or $H_2O$ were obtained under excitation at $\lambda = 980$ nm (15 W cm$^{-2}$) with a laser diode ($\lambda = 980$ nm, CNI, MDL-*N*-980) coupled to a Fluorometer FluoroLog (Horiba). The laser-power density was measured as described above.

### TEM

TEM images were collected for core-$NaYF_4$:Yb/Tm, core@shell-NaYF4:Yb/Tm@$NaYF_4$, and **UCNP@4** samples on a JEOL JEM-1400 PLUS-HC microscope that operated at 120 kV. A small amount of the sample was dispersed in $H_2O$ or THF (1 mL) as the solvent to give an approximate 0.5 mg mL$^{-1}$ solution. One drop (3 μL) of the resulting solution was allowed to evaporate on a carbon film supported on a 300 mesh copper grid (diameter = 3 mm).

### XPS

XPS data of **4** and **UCNP@4** were acquired on a SPECS Sage HR 100 spectrometer with a non-monochromatic X-ray source ($Mg_{K\alpha}$ of 1253.6 eV) and an applied power of 250 W. The spectrometer was calibrated by using the $3d_{5/2}$ line of Ag with a full width at half maximum (FWHM) of 1.1 eV. All the measurements were made in an ultrahigh vacuum (UHV) chamber at a pressure below $8{\cdot}10^{-8}$ mbar. The samples were measured on titanium surfaces.

### UPLC-MS

UPLC-MS measurements on **1**–**4** were performed by using positive-ion electrospray ionisation mass spectrometry (ESI-MS) on a LCT Premier XE machine (resolution: 10000 FWHM) from Waters coupled to an ultraperformance liquid chromatograph. Samples were prepared in a $H_2O$/DMSO (95:5%) mixture. The analysis was achieved on an Acquity UPLC BEH C18 column (50×2.1 mm) with $H_2O$ (0.1% formic acid)/MeOH as the mobile phase at a flow rate of 0.3 mL min$^{-1}$ and an injection volume of 5 μL. The ESI source was employed in the W-optics positive-ionisation scan mode with the capillary voltage at 2.5 kV. The temperatures of the source and desolvation were 120 °C. The cone and desolvation gas flows were 50 and 600 L h$^{-1}$. The collision gas flow was 0.2 mL min$^{-1}$ and a collision energy of 15–18 V was applied. Sonicated and ultracentrifugation ($10^5$ rpm, 45 min) was used in the case of **UCNP@4** to eliminate possible aggregates and nanoparticles before injection for UPLC-MS.

### Ligand-photodissociation quantum yield

The quantum yields ($\Phi$) of ligand photodissociation were determined for **1** and **2** in $H_2O$ upon excitation at $\lambda = 395$ nm. UV/Vis absorption spectroscopy was employed to quantify the formation of the photoproducts as function of irradiation time (nmol s$^{-1}$). At the same time, ferrioxalate actinometer $K_3[Fe(C_2O_4)_3]$ was used to determine the photon flux (μmol s$^{-1}$) on the samples exposed to the Prizmatix LED Multiwavelength MWLLS-11 at $\lambda = 395$ nm. Full details are given in the Supporting Information. Complex $K_3[Fe(C_2O_4)_3]$ was obtained by following the procedure described by Carriazo.[53]

### Computational details

All the calculations were performed with the Gaussian 09 (G09) program package,[54] which employed DFT and TD-DFT methods,[55,56] the Becke three-parameter hybrid functional,[57] and the Lee–Yang–Parr gradient-corrected correlation functional (B3LYP).[58] The solvent effect was included by using the polarizable continuum model (PCM)[59,60] with water as the solvent. The LanL2DZ basis set[61] and effective core potential were used for the Ru atom and the 6-31G** basis set[62] was used for all the other atoms. The B3LYP/LanL2DZ/6–31G** combination was selected because it had previously provided satisfactory results for similar ruthenium–arene complexes.[35,36]

Geometry optimisations of the ground states (S0) and the lowest-lying triplet states (T0 and T1) for **1** and **2** were carried out without any symmetry constraints. The nature of all the stationary points was verified by using harmonic vibrational frequency calculations. No imaginary frequencies were found, thus indicating we had located the minima on the potential-energy surfaces.

The UV/Vis electronic absorption spectra were simulated by using TD-DFT,[55,56] in which a total of 50 singlet excited states were computed. The electronic distribution and the localisation of the singlet excited states were visualised by using electron-density difference maps (EDDMs).

GaussSum 2.2.5[63] was used to simulate the theoretical UV/Vis spectra and for extraction of EDDMs.[64,65] Molecular-graphic images were produced by using the UCSF Chimera package from the Re-

source for Biocomputing, Visualization, and Informatics at the University of California, San Francisco (supported by NIH P41 RR001081).[66] A full summary of the computational results is reported in the Supporting Information.

## Acknowledgements

Our work in this area was supported by the Spanish Ministry of Economy and Competitiveness (grant CTQ2012-39315), the Department of Industry of the Basque Country (grant ETORTEK). L.S. and E.R. were supported by the MICINN of Spain with the Ramón y Cajal Fellowship RYC-2011-07787 and by the MC CIG fellowship UCnanomat4iPACT (grant no. 321791). We gratefully acknowledge Ikerbasque for the Visiting Professor Fellowship to A.H. and members of the European COST Actions CM1105 and CM1403 for stimulating discussions. Marco Moller, Javier Calvo, Daniel Padró, and Luis Yate are also kindly acknowledged for help in the collection of experimental data. Moreover, technical and human support provided by SGIker (UPV/EHU, MINECO, GV/EJ, ERDF, and ESF) is gratefully acknowledged.

**Keywords:** nanoparticles · near-infrared radiation · photoactivation · ruthenium · upconversion

[1] D. E. J. G. J. Dolmans, D. Fukumura, R. K. Jain, *Nat. Rev. Cancer* **2003**, *3*, 380 – 387.
[2] E. Fino, R. Araya, D. S. Peterka, M. Salierno, R. Etchenique, R. Yuste, *Front. Neural Circuits* **2009**, *3*, 2.
[3] M. A. Sgambellone, A. David, R. N. Garner, K. R. Dunbar, C. Turro, *J. Am. Chem. Soc.* **2013**, *135*, 11274 – 11282.
[4] U. Schatzschneider, *Eur. J. Inorg. Chem.* **2010**, 1451 – 1467.
[5] E. Ruggiero, S. Alonso-de Castro, A. Habtemariam, L. Salassa, *Struct. Bonding* **2015**, *165*, 69 – 108.
[6] N. J. Farrer, L. Salassa, P. J. Sadler, *Dalton Trans.* **2009**, 10690 – 10701.
[7] E. C. Glazer, *Isr. J. Chem.* **2013**, *53*, 391 – 400.
[8] D. Barolet, *Semin. Cutan. Med. Surg.* **2008**, *27*, 227 – 238.
[9] Z. Chen, W. Sun, H. J. Butt, S. Wu, *Chem. Eur. J.* **2015**, *21*, 9165 – 9170.
[10] E. Wachter, D. K. Heidary, B. S. Howerton, S. Parkin, E. C. Glazer, *Chem. Commun.* **2012**, *48*, 9649 – 9651.
[11] M. J. Rose, P. K. Mascharak, *Inorg. Chem.* **2009**, *48*, 6904 – 6917.
[12] M. J. Rose, N. L. Fry, R. Marlow, L. Hinck, P. K. Mascharak, *J. Am. Chem. Soc.* **2008**, *130*, 8834 – 8846.
[13] J. V. Garcia, J. Yang, D. Shen, C. Yao, X. Li, R. Wang, G. D. Stucky, D. Zhao, P. C. Ford, F. Zhang, *Small* **2012**, *8*, 3800 – 3805.
[14] A. E. Pierri, P.-J. Huang, J. V. Garcia, J. G. Stanfill, M. Chui, G. Wu, N. Zheng, P. C. Ford, *Chem. Commun.* **2015**, *51*, 2072 – 2075.
[15] P. T. Burks, J. V. Garcia, R. Gonzalezlrias, J. T. Tillman, M. Niu, A. A. Mikhailovsky, J. Zhang, F. Zhang, P. C. Ford, *J. Am. Chem. Soc.* **2013**, *135*, 18145 – 18152..
[16] E. Ruggiero, A. Habtemariam, L. Yate, J. C. Mareque-Rivas, L. Salassa, *Chem. Commun.* **2014**, *50*, 1715 – 1718.
[17] E. Ruggiero, J. Hernandez-Gil, J. C. Mareque-Rivas, L. Salassa, *Chem. Commun.* **2015**, *51*, 2091 – 2094.
[18] S. Wu, H. J. Butt, *Adv. Mater.* **2015**, DOI: 10.1002/adma.201502843.
[19] Z. Chen, S. He, H. J. Butt, S. Wu, *Adv. Mater.* **2015**, *27*, 2203 – 2206.
[20] S. He, K. Krippes, S. Ritz, Z. Chen, A. Best, H. J. Butt, V. Mailänder, S. Wu, *Chem. Commun.* **2015**, *51*, 431 – 434.
[21] M. Haase, H. Schäfer, *Angew. Chem. Int. Ed.* **2011**, *50*, 5808 – 5829; *Angew. Chem.* **2011**, *123*, 5928 – 5950.
[22] J. Zhou, Q. Liu, W. Feng, Y. Sun, F. Li, *Chem. Rev.* **2015**, *115*, 395 – 465.
[23] S. H. C. Askes, A. Bahreman, S. Bonnet, *Angew. Chem. Int. Ed.* **2014**, *53*, 1029 – 1033; *Angew. Chem.* **2014**, *126*, 1047 – 1051.
[24] Y. Sun, M. Yu, S. Liang, Y. Zhang, C. Li, T. Mou, W. Yang, X. Zhang, B. Li, C. Huang, F. Li, *Biomaterials* **2011**, *32*, 2999 – 3007.
[25] T. Cao, Y. Yang, Y. Sun, Y. Wu, Y. Gao, W. Feng, F. Li, *Biomaterials* **2013**, *34*, 7127 – 7134.
[26] J.-W. Shen, C.-X. Yang, L.-X. Dong, H.-R. Sun, K. Gao, X.-P. Yan, *Anal. Chem.* **2013**, *85*, 12166 – 12172.
[27] J. Zhou, Y. Sun, X. Du, L. Xiong, H. Hu, F. Li, *Biomaterials* **2010**, *31*, 3287 – 3295.
[28] L. Xiong, Z. Chen, Q. Tian, T. Cao, C. Xu, F. Li, *Anal. Chem.* **2009**, *81*, 8687 – 8694.
[29] S. K. Maji, S. Sreejith, J. Joseph, M. Lin, T. He, Y. Tong, H. Sun, S. W.-K. Yu, Y. Zhao, *Adv. Mater.* **2014**, *26*, 5632 – 5632.
[30] Y. Sun, W. Feng, P. Yang, C. Huang, F. Li, *Chem. Soc. Rev.* **2015**, *44*, 1509 – 1525.
[31] J. Zhou, Z. Liu, F. Li, *Chem. Soc. Rev.* **2012**, *41*, 1323 – 1349.
[32] G. Gasser, I. Ott, N. Metzler-Nolte, *J. Med. Chem.* **2011**, *54*, 3 – 25.
[33] Z. Adhireksan, G. E. Davey, P. Campomanes, M. Groessl, C. M. Clavel, H. Yu, A. A. Nazarov, C. H. F. Yeo, W. H. Ang, P. Dröge, U. Rothlisberger, P. J. Dyson, C. A. Davey, *Nat. Commun.* **2014**, *5*, 3462.
[34] M. Frik, A. Martínez, B. T. Elie, O. Gonzalo, D. Ramírez de Mingo, M. Sanaú, R. Sánchez-Delgado, T. Sadhukha, S. Prabha, J. W. Ramos, I. Marzo, M. Contel, *J. Med. Chem.* **2014**, *57*, 9995 – 10012.
[35] S. Betanzos-Lara, L. Salassa, A. Habtemariam, O. Novakova, A. M. Pizarro, G. J. Clarkson, B. Liskova, V. Brabec, P. J. Sadler, *Organometallics* **2012**, *31*, 3466 – 3479.
[36] S. Betanzos-Lara, L. Salassa, A. Habtemariam, P. J. Sadler, *Chem. Commun.* **2009**, 6622 – 6624.
[37] G. Ragazzon, I. Bratsos, E. Alessio, L. Salassa, A. Habtemariam, R. J. McQuitty, G. J. Clarkson, P. J. Sadler, *Inorg. Chim. Acta* **2012**, *393*, 230 – 238.
[38] J.-C. Boyer, M.-P. Manseau, J. I. Murray, F. C. J. M. van Veggel, *Langmuir* **2010**, *26*, 1157 – 1164.
[39] R. A. Zelonka, M. C. Baird, *Can. J. Chem.* **1972**, *50*, 3063 – 3072.
[40] M. A. Bennett, A. K. Smith, *J. Chem. Soc. Dalton Trans.* **1974**, 233 – 241.
[41] A. Habtemariam, M. Melchart, R. Fernández, S. Parsons, I. D. H. Oswald, A. Parkin, F. P. A. Fabbiani, J. E. Davidson, A. Dawson, R. E. Aird, D. I. Jodrell, P. J. Sadler, *J. Med. Chem.* **2006**, *49*, 6858 – 6868.
[42] F. Wang, A. Habtemariam, E. P. L. van der Geer, R. Fernández, M. Melchart, R. J. Deeth, R. Aird, S. Guichard, F. P. A. Fabbiani, P. Lozano-Casal, I. D. H. Oswald, D. I. Jodrell, S. Parsons, P. J. Sadler, *Proc. Natl. Acad. Sci. U. S. A.* **2005**, *102*, 18269 – 18274.
[43] B. S. Uppal, A. Zahid, P. I. P. Elliott, *Eur. J. Inorg. Chem.* **2013**, 2571 – 2579.
[44] B. C. Boren, S. Narayan, L. K. Rasmussen, L. Zhang, H. Zhao, Z. Lin, G. Jia, V. V. Fokin, *J. Am. Chem. Soc.* **2008**, *130*, 8923 – 8930.
[45] J.-C. Boyer, C.-J. Carling, S. Y. Chua, D. Wilson, B. Johnsen, D. Baillie, N. R. Branda, *Chem. Eur. J.* **2012**, *18*, 3122 – 3126.
[46] L.-L. Li, P. Wu, K. Hwang, Y. Lu, *J. Am. Chem. Soc.* **2013**, *135*, 2411 – 2414.
[47] A. K. Tucker-Schwartz, R. L. Garrell, *Chem. Eur. J.* **2010**, *16*, 12718 – 12726.
[48] M. Montalti, A Credi, L Prodi, M. T. Gandolfi, *Handbook of Photochemistry*, 3rd ed., CRC, Boca Raton, **2006**.
[49] F. Vetrone, R. Naccache, V. Mahalingam, C. G. Morgan, J. A. Capobianco, *Adv. Funct. Mater.* **2009**, *19*, 2924 – 2929.
[50] J.-C. Boyer, C.-J. Carling, B. D. Gates, N. R. Branda, *J. Am. Chem. Soc.* **2010**, *132*, 15766 – 15772.
[51] C. J. Carling, F. Nourmohammadian, J. C. Boyer, N. R. Branda, *Angew. Chem. Int. Ed.* **2010**, *49*, 3782 – 3785; *Angew. Chem.* **2010**, *122*, 3870 – 3873.
[52] N. Bogdan, F. Vetrone, G. A. Ozin, J. A. Capobianco, *Nano Lett.* **2011**, *11*, 835 – 840.
[53] J. G. Carriazo, Khimiya **2010**, *19*, 103 – 112.
[54] Gaussian 09 (Revision C.01), M. J. Frisch, G. W. Trucks, H. B. Schlegel, G. E. Scuseria, M. A. Robb, J. R. Cheeseman, G. Scalmani, V. Barone, B. Mennucci, G. A. Petersson, H. Nakatsuji, M. Caricato, X. Li, H. P. Hratchian, A. F. Izmaylov, J. Bloino, G. Zheng, J. L. Sonnenberg, M. Hada, M. Ehara, K. Toyota, R. Fukuda, J. Hasegawa, M. Ishida, T. Nakajima, Y. Honda, O. Kitao, H. Nakai, T. Vreven, J. A. Montgomery, Jr., J. E. Peralta, F. Ogliaro, M. Bearpark, J. J. Heyd, E. Brothers, K. N. Kudin, V. N. Staroverov, R. Kobayashi, J. Normand, K. Raghavachari, A. Rendell, J. C. Burant, S. S. Iyengar, J. Tomasi, M. Cossi, N. Rega, J. M. Millam, M. Klene, J. E. Knox, J. B. Cross, V. Bakken, C. Adamo, J. Jaramillo, R. Gomperts, R. E. Stratmann, O. Yazyev, A. J. Austin, R. Cammi, C. Pomelli, J. W. Ochterski, R. L.

 

Martin, K. Morokuma, V. G. Zakrzewski, G. A. Voth, P. Salvador, J. J. Dannenberg, S. Dapprich, A. D. Daniels, Ö. Farkas, J. B. Foresman, J. V. Ortiz, J. Cioslowski, D. J. Fox, Gaussian, Inc.: Wallingford, CT, **2009**.
[55] M. E. Casida, C. Jamorski, K. C. Casida, D. R. Salahub, *J. Chem. Phys.* **1998**, *108*, 4439 – 4449.
[56] R. E. Stratmann, G. E. Scuseria, M. J. Frisch, *J. Chem. Phys.* **1998**, *109*, 8218 – 8224.
[57] A. D. Becke, *J. Chem. Phys.* **1993**, *98*, 5648 – 5652.
[58] C. Lee, W. Yang, R. G. Parr, *Phys. Rev. B* **1988**, *37*, 785 – 789.
[59] M. Cossi, G. Scalmani, N. Rega, V. Barone, *J. Chem. Phys.* **2002**, *117*, 43 – 54.
[60] S. Miertuš, E. Scrocco, J. Tomasi, *Chem. Phys.* **1981**, *55*, 117 – 129.
[61] P. J. Hay, W. R. Wadt, *J. Chem. Phys.* **1985**, *82*, 270 – 283.
[62] A. D. McLean, G. S. Chandler, *J. Chem. Phys.* **1980**, *72*, 5639 – 5648.
[63] N. M. O'Boyle, A. L. Tenderholt, K. M. Langner, *J. Comput. Chem.* **2008**, *29*, 839 – 845.
[64] W. R. Browne, N. M. O'Boyle, J. J. McGarvey, J. G. Vos, *Chem. Soc. Rev.* **2005**, *34*, 641 – 663.
[65] M. Head-Gordon, A. M. Grana, D. Maurice, C. A. White, *J. Phys. Chem.* **1995**, *99*, 14261 – 14270.
[66] E. F. Pettersen, T. D. Goddard, C. C. Huang, G. S. Couch, D. M. Greenblatt, E. C. Meng, T. E. Ferrin, *J. Comput. Chem.* **2004**, *25*, 1605 – 1612.

Received: October 6, 2015
Published online on January 19, 2016

 